Computers and Mathematics with Applications 79 (2020) 2872–2884

Contents lists available at ScienceDirect

Computers and Mathematics with Applications

journal homepage: www.elsevier.com/locate/camwa

Method of analytical regularization in the analysis of axially symmetric excitation of imperfect circular disk antennas

Nataliya Y. Saidoglu (Ph.D.) [a], Alexander I. Nosich [b,*]

[a] Stellar Solutions Inc., 250 Cambridge Ave #204, Palo Alto, CA 94306, USA
[b] Institute of Radio-Physics and Electronics NASU, Kharkiv 61085, Ukraine

ARTICLE INFO

Article history:
Received 6 May 2019
Received in revised form 27 November 2019
Accepted 19 December 2019
Available online 2 January 2020

Keywords:
Disk antenna
Generalized boundary condition
Singular integral equations
Fredholm second kind matrix equation

ABSTRACT

This work presents accurate numerical method and computational results in the modeling of the axisymmetric radiation of resistive and thin-dielectric circular disk-on-substrate antennas. To simulate resistive and thin-dielectric disk features, we use two-side Generalized Boundary Conditions (GBC). The analysis is based on the singular integral equations (IEs) and the Method of Analytical Regularization (MAR) exploiting a Galerkin Method (GM) with judicious basis functions, which convert IEs into the Fredholm second-kind infinite matrix equations. Unlike previously known numerical techniques, this guarantees convergence and enables us to compute the solution with controlled accuracy even in sharp resonances. Numerical results demonstrate the effect of disk losses and transparency on the fundamental radiation phenomena and help improve antenna characteristics such as radiation efficiency.

1. Introduction

Circular metallic disk is a canonic scatterer in computational electromagnetics. In part, this is because such disks are widely used in microwave communications and radar as microstrip antenna array elements [1]. Single circular disks on substrates are able to produce conical patterns [2] and are used as horizontally omnidirectional cellular and automobile antennas [3]. Resistive patches are attractive as more broadband antennas [4]. Moreover, recent appearance of new technologies has made available low-loss and high-permittivity dielectric disk antennas [5–7], which may have some advantages.

Numerical tools of disk antenna design consist of direct-numerical and numerical–analytical methods such as finite-difference-time domain (FDTD) and method of moments (MM). FDTD is used to study many electromagnetic problems including inverse and time-domain ones. However, its application to antennas entails severe difficulties in how to limit the infinite space domain and how to mesh it properly. This leads to the violation of the radiation condition and also to very large-size matrices to be inverted. In contrast, MM is based on a numerical approximation of IEs derived for the equivalent currents. Although less flexible than FDTD, it is more economic. This is because only the boundaries need to be discretized, while the radiation condition is automatically satisfied due to the proper choice of the IE kernels. In the 1980's, numerous remarkable MM analyses of perfectly electric conducting (PEC) circular disk antennas were published [8–13]. Thanks to the rotational symmetry, they worked mainly with the Hankel-transformed IEs and used transforms of so-called "cavity modes" as basis functions.

* Corresponding author.
E-mail addresses: lukyasha2003@yahoo.com (N.Y. Saidoglu), anosich@yahoo.com (A.I. Nosich).

https://doi.org/10.1016/j.camwa.2019.12.020
0898-1221/

However, electromagnetic problems are mostly reduced to the first-kind and/or strongly singular IEs, and thus the convergence of common MM algorithms, which end up with the dense matrices, generally cannot be guaranteed [14]. Especially significant losses of accuracy in MM and FDTD may happen near the sharp resonances [15]. As printed antennas are essentially resonant devices, this disadvantage is quite serious. Additionally, both MM and FDTD are time and memory consuming even for obtaining basic results. If the frequency is increased, the required computer resources rapidly grow up. Therefore, the modeling in wide band and its numerical optimization is painful, especially if a supercomputer is not available.

Although today there is no versatile theoretical technique able to compute arbitrary patch antennas with arbitrary accuracy, it is possible to achieve this goal in the case of circular disks, both PEC and imperfect. Such a study can be valuable for a better insight in the fundamental wave phenomena in patch antennas in general. For example, the effect of the patch partial transparency and losses on the antenna characteristics has not been well quantified yet. Provided that the dielectric disk thickness is a fraction of the wavelength, one may derive open-surface IEs either by using generalized boundary conditions (GBC) and Green's theorems [16,17] or via reduction from the volume IEs [18,19].

Rapidly convergent IE algorithms can be built by using the concept of analytical regularization, which implies an equivalent transformation of the original singular IE (or a set of them) to the Fredholm second-kind matrix equation, with or without the intermediate stage of a Fredholm second-kind IE having a smooth kernel (see [20]). In contrast to other techniques, the power of the Fredholm second-kind equations is in the existence of unique solution of infinite matrix equation and guaranteed convergence of numerical approximations. The first application of MAR to a PEC circular disk was done in [21,22].where the dual IEs in the Hankel Transform domain were considered instead of the singular IEs. They were transformed to Fredholm second-kind IEs and then numerically solved by the collocation algorithm (pulse basis — delta testing, in MM terminology). Alternatively, in [23] it was proposed to solve the same dual IEs by using MAR in the form of specialized GM. By using the latter technique, radiation characteristics of an axisymmetrically excited PEC circular-disk antenna were studied in [24]. Similar ideas can be found behind the developed later weighted-Chebyshev GM [22] and Neumann-series GM [25–30].

For the sake of completeness, it should be also mentioned that rapidly convergent numerical solutions to electromagnetics IEs with smooth and singular kernels can be obtained using the Nystrom-type algorithms [31–33]. Such algorithms do not use partial inversion and, instead, rely on the theorems of approximation of integrals with quadratures. Their numerical performance is generally at the same level as those based on MAR although, unlike Fredholm second-kind IE, they cannot be used for obtaining analytic solutions in the form of asymptotic series in quasi-static limit.

In this paper, the static-eigenfunction-GM version of MAR is generalized for the analysis of axisymmetrically excited circular-disk resistive and thin-dielectric antennas on infinite dielectric grounded substrates. Some of numerical results have been presented in the conference paper [34]; here the full theory is presented and dielectric-disk case is added. Section 2 contains mathematical formulations. In Section 3, we solve singular IEs of two auxiliary problems about a resistive disk in free space excited by vertical electric and magnetic dipoles (VED and VMD) and show connections between singular IE and dual IE. Sections 4 and 5 present MAR-based analyses of resistive and thin dielectric disk antennas, respectively. In Section 6, numerical results are presented followed by the Conclusions.

2. Formulation and GBC

Fig. 1 shows the geometry of the problem. A disk of the thickness b and radius a can be resistive with finite electron conductivity σ or dielectric with dielectric permittivity $\varepsilon_d\varepsilon_0$, $\varepsilon_d = \varepsilon_d' + i\varepsilon_d''$. It is placed on an infinite dielectric substrate of the thickness h and real-valued dielectric permittivity $\varepsilon_0\varepsilon$ backed with a PEC ground plane. This structure is excited by the given VED current, $\boldsymbol{J}^e$, located in the origin of cylindrical coordinates (r, φ, z) that is on the ground plane below the disk center. The time dependence is assumed to be $\exp(i\omega t)$, where ω is the angular frequency (this factor will be suppressed throughout the paper). Free-space and substrate-material wavenumbers are $k_0 = \omega\sqrt{\varepsilon_0\mu_0} = 2\pi/\lambda_0$ and $k_\varepsilon = k_0\sqrt{\varepsilon_d} = 2\pi/\lambda_\varepsilon$, respectively.

The problem consists in determination of the total electromagnetic field $\{\vec{E}, \vec{H}\}$, which satisfies *inhomogeneous Maxwell's equations* with a piecewise-constant permittivity ε, *continuity conditions* for the tangential components at the substrate interface, *PEC boundary condition* at the ground plane, and *modified radiation condition* at $r \to \infty$ that takes into account both the spherical wave and the surface waves of the substrate [35]. Besides, the field must satisfy certain boundary conditions on the disk. As known, if a penetrable sheet is thin, $b \ll \lambda_0$, one can exclude the internal field from consideration by assuming the thickness to be zero however imposing certain effective two-side GBC [16,17]. In the resistive disk case, we use GBC for a thinner-than-skindepth metal sheet:

$$\frac{1}{2}\left[\boldsymbol{E}_t^\varepsilon + \boldsymbol{E}_t^0\right] = Z_0 R\boldsymbol{n} \times \left[\boldsymbol{H}_t^\varepsilon - \boldsymbol{H}_t^0\right], \tag{1}$$

$$\boldsymbol{E}_t^\varepsilon = \boldsymbol{E}_t^0, \tag{2}$$

where the indices 0 and ε refer to the free half-space and dielectric substrate, respectively, $\boldsymbol{n}$ is the unit-normal vector oriented along the z-axis, subscript «t» means "tangential", $Z_0 = (\mu_0/\varepsilon_0)^{1/2}$ is the free-space impedance, $R = (Z_0 b\sigma)^{-1}$ is the normalized electrical resistivity [16], and σ is the electron conductance.

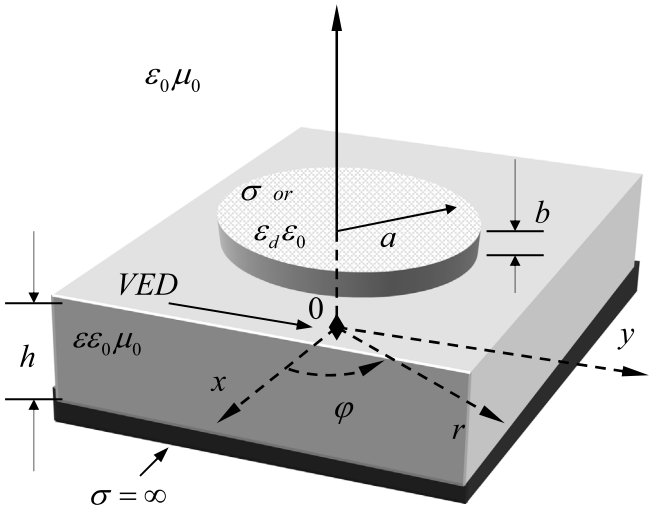

Fig. 1. Geometry of circular disk-on-substrate scatterer axisymmetrically excited by VED.

For the simulation of a thin dielectric disk, we use GBC in the following form [17]:

$$\frac{1}{2}\left[\boldsymbol{E}_t^{\varepsilon} + \boldsymbol{E}_t^{0}\right] = Z_0 R_d \boldsymbol{n} \times \left[\boldsymbol{H}_t^{\varepsilon} - \boldsymbol{H}_t^{0}\right], \tag{3}$$

$$\frac{1}{2}\left[\boldsymbol{H}_t^{\varepsilon} + \boldsymbol{H}_t^{0}\right] = -Z_0^{-1} S_d \boldsymbol{n} \times \left[\boldsymbol{E}_t^{\varepsilon} - \boldsymbol{E}_t^{0}\right], \tag{4}$$

where R_d and S_d are the normalized electrical and magnetic resistivities, respectively. In the case of a single-layer sheet having $|\varepsilon_d| \gg 1$ and $b \ll \lambda_0$, they can be found in closed form from the plane-wave scattering by infinite sheet [17],

$$R_d = \frac{i}{2}\varepsilon_d^{-1/2} \cot\left(\frac{1}{2}\varepsilon_d^{1/2} k_0 b\right), \quad S_d = \frac{i}{2}\varepsilon_d^{1/2} \cot\left(\frac{1}{2}\varepsilon_d^{1/2} k_0 b\right), . \tag{5}$$

Although these GBC are derived for an infinite flat thin sheet, we shall apply them for finite disks. As remarked in [16], using GBC is less ambiguous than using together PEC conditions and zero thickness of a screen. Besides, we shall include an appropriate *edge condition* into the problem formulation that is a request that the field power is finite in any bounded domain including domain containing the disk rim. This set of conditions guarantees the uniqueness of the disk antenna problem solution.

Note that in the resistive-disk case, the edge condition entails that the normal component of the current vanishes as $(a - r)^{1/2}$ at the rim and the parallel component is finite [36].

3. Singular IEs and solution by MAR

3.1. Hyper-singular IE for a VED-excited resistive disk in free space

Consider now an auxiliary scattering problem of a resistive disk, which is placed in free space at the plane $z = 0$ and axisymmetrically excited by a VED. Decompose the total electromagnetic field $\{\boldsymbol{E}, \boldsymbol{H}\}$ into a sum of the incident field $\{\boldsymbol{E}^{in}, \boldsymbol{H}^{in}\}$ generated by the given current in the host medium without the disk, and the scattered field $\{\boldsymbol{E}^{sc}, \boldsymbol{H}^{sc}\}$ excited by the currents induced on the disk. In the axisymmetric problems, the fields can be conveniently derived via either H_φ of E_φ component. In the case considered, this enables one to look for the scattered field as a generalized double-layer potential:

$$H_\varphi(r, z) = \int_0^a j_r(r') \frac{\partial}{\partial z'} G^0(r, r', z, z')\, r' dr' \Big|_{z'=0}, \tag{6}$$

where

$$G^0(r, r', z, z') = \int_0^{2\pi} \frac{\exp(-ik_0 R_{pq})}{R_{pq}} \cos\psi\, d\psi, \tag{7}$$

$$R_{pq} = [(z - z')^2 + r^2 + r'^2 - 2rr' \cos\psi]^{1/2}, \tag{8}$$

$p = (r, z)$ and $q = (r', z')$ are the observation and source points, respectively, and $j_r(r)$ is the surface current to be found. The function (7) is the so-called first-order modal Green's function (see [32] and references therein), appearing in the

process of expansion of the 3-D Green's function $\exp(-ik_0R_{pq})/R_{pq}$ in terms of Fourier series in azimuth. Then GBC (1), (2) lead to the following IE:

$$ik_0Rj_r(r)+\int_0^a j_r(r')\frac{\partial^2}{\partial z\partial z'}G^0(r,r',z,z')\,r'dr'=ik_0Z_0^{-1}E_r^{in}(r), \tag{9}$$

where $z=z'=0$ and E_r^{in} is a known function of excitation.

If $r\to r'$, the function $K(r,r')=\left.\frac{\partial^2 G^0(r,r',z,z')}{\partial z\partial z'}\right|_{z,z'=0}$ asymptotically behaves as

$$K(r,r')=K_{st}(r,r')+2k_0^2\left[r^{-1}\ln\xi+O(1)\right], \tag{10}$$

where $\xi=r/(r-r')$, and the first, i.e. the static, term can be reduced to the elliptic functions showing that

$$K_{st}(r,r')=\frac{\partial}{\partial z}\frac{\partial}{\partial z'}\int_0^{2\pi}\frac{\cos\psi}{R_{pq}}d\psi\underset{r\to r'}{\sim}\frac{2}{r^3}\left(\xi^2-\frac{3}{8}\ln\xi\right), \tag{11}$$

Thus, it is seen that IE (9) is hyper-singular, with the dominant singularity provided by the static part of kernel, and should be understood in Hadamard principal-part sense. Hence, although it is a second kind IE for any $R\neq 0$, this is not a Fredholm equation. As a result, convergence of its numerical solution through usual MM discretization schemes (e.g., pulse basis — delta testing) is not guaranteed, because they end up with ill-conditioned matrix equations. Therefore, we shall develop a MAR, which converts "bad" IE (9) into a "good" Fredholm second-kind matrix equation.

3.2. Eigenfunctions of the IE operator static limit for VED-excited PEC and resistive disks

In the wave scattering by PEC and imperfect thin screens, MAR is based on the analytical inversion of the static parts of IEs (see [20]). It is possible to combine regularization and discretization of a singular IE like (9) in a single operation. To do this, the GM basis functions should be orthogonal eigenfunctions of the most singular part of the IE operator. Consider the functions defined as

$$\Phi_n(s)=\begin{cases}\varsigma_n s\mathrm{P}_n^{(1,1/2)}\left(1-2s^2\right), & s\le 1\\ 0, & s>1\end{cases}, \tag{12}$$

where we have introduced dimensionless coordinate $s=r/a$, $n=0,1,\ldots,\varsigma_n=n!(2n+5/2)^{1/2}\Gamma^{-1}(n+3/2)$, and $\mathrm{P}_n^{(1,1/2)}(.)$ is a conventional Jacobi polynomial. In the considered case of axisymmetrically VED-excited circular disk, these functions are the eigenfunctions of static limit of singular integral operator of (9), with the weight $w(s)=(1-s^2)^{1/2}$. Namely,

$$\int_0^1 w(s')\Phi_n(s')K_{st}(s,s')\,s'ds'=\mu_n\Phi_n(s), \tag{13}$$

where $\mu_n=2\Gamma(n+3/2)\Gamma(n+5/2)(n!(n+1)!)^{-1}$. The orthogonality of the functions (12) is given by

$$\int_0^1 w(s)\Phi_n(s)\Phi_p(s)\,sds=\mu_n^{-1}\delta_{np}, \tag{14}$$

where δ_{np} is the Kronecker delta. Further, define direct and inverse Hankel Transforms of the first order as

$$f(\kappa)=\kappa\int_0^\infty g(s)J_1(\kappa s)\,sds, \tag{15}$$

$$g(s)=\int_0^\infty f(\kappa)J_1(\kappa s)\,d\kappa, \tag{16}$$

respectively. The Hankel Transform images of the weighted functions (12) can be then derived in the closed form as

$$\int_0^\infty w(s)\Phi_n(s)J_1(\kappa s)\,sds=\frac{\phi_n(\kappa)}{\kappa}, \tag{17}$$

$$\phi_n(\kappa)=\eta_n\kappa^{-1/2}J_{2n+5/2}(\kappa),\quad 0\le\kappa<\infty, \tag{18}$$

$\eta_n=(4n+5)^{1/2}$, and $J_{2n+5/2}(\kappa)$ is the Bessel function. The orthogonality relation in the transform domain is given by

$$\int_0^\infty \phi_n(\kappa)\phi_p(\kappa)d\kappa=\delta_{np}. \tag{19}$$

The functions (18) were first used as full-wave GM basis in [23] because of the following properties: they are complete and orthogonal on the interval $0<\kappa<\infty$, and their originals satisfy the edge condition at $s\to 1$. Now we shall see that their role is even more important as they invert the static (most singular) part of associated dual IE. As can be seen from (9), zero resistivity of the disk does not change the singular part of IE operator. Thus, the discussed basis functions can be used both in PEC and resistive-disk cases.

3.3. Matrix equation and dual IE for a VED-excited disk

In order to discretize and partially invert IE (9) we expand the disk current in terms of the weighted functions (12) as

$$j_r(s) = w(s)\sum_{n=0}^{\infty} x_n \Phi_n(s), \tag{20}$$

where x_n are unknown coefficients. Taking advantage of (10) and (13), we test IE with each of the function $w(s)\Phi_p(s)$ and use (14) to come to the following matrix equation:

$$x_p + \sum_{n=0}^{\infty} x_n \tilde{A}_{np} = \tilde{B}_p, \quad p = 0, 1, 2 \ldots \infty, \tag{21}$$

$$A_{np} = \int_0^1 \int_0^1 w w' \Phi_p \Phi_n' \left[K(s,s') - K_{st}(s,s') + ik_0 aR\delta(s-s')\right] ss' ds ds', \tag{22}$$

$$\tilde{B}_p = ik_0 Z_0^{-1} \int_0^1 E_r^{in}(s)\, w(s)\, \Phi_p(s)\, s ds, \tag{23}$$

where primed quantities depend on the primed argument. Large-index behavior of the elements (22) is established as $O[(pn)^{1/2}(n^4+p^4)^{-1}]$. Hence the corresponding operator is compact (i.e., has a bounded l_2-norm: $\|\tilde{A}\|_{l_2}^2 = \sum_{p,n} |\tilde{A}_{pn}|^2 < \infty$). As the column-vector (23) belongs to the same space l_2, matrix equation (21) is a Fredholm second kind one.

Now we will show the connection between the hyper-singular IEs and the dual IEs, frequently used in disk scattering problems [9,10,12,23–26,37]. By using the known representation of the axisymmetric free-space Green's function,

$$G^0(s,s') = (4\pi)^{-1} \int_0^{\infty} \gamma_0^{-1}(\kappa) e^{\gamma_0 |z-z'|/a} J_1(\kappa s) J_1(\kappa s') \kappa d\kappa, \tag{24}$$

where $\gamma_0(\kappa) = (\kappa^2 - k_0^2 a^2)^{1/2}$, we obtain that

$$K(s,s') = \int_0^{\infty} \gamma_0(\kappa) J_1(\kappa s) J_1(\kappa s') \kappa d\kappa. \tag{25}$$

On continuing $j_r(s)$ by zero value out of the disk region, the substitution of (20), (17) and (25) into (9) and integration with respect to r' over the whole domain yields dual IE as

$$\begin{cases} \int_0^{\infty} X(\kappa)[\gamma_0(\kappa) + ik_0 aR] J_1(\kappa s)\, d\kappa = ik_0 Z_0^{-1} E_r^{in}(s), & s \le 1 \\ \int_0^{\infty} X(\kappa) J_1(\kappa s)\, d\kappa = 0, & s > 1 \end{cases}. \tag{26}$$

Here $X(\kappa)$ is the Hankel Transform of the "extended" $j_r(r)$, therefore

$$X(\kappa) = \sum_{n=0}^{\infty} x_n \phi_n(\kappa) \tag{27}$$

and we apply the operator $\int_0^{\infty} w(s)\Phi_p(s) s ds$ to both sides of (26). The second equation in (26), due to the properties of the basis functions, is satisfied automatically [38]. As for the first equation, its *static limit* is solved explicitly. Indeed, a study of the function $\gamma_0(\kappa)$ behavior if $\kappa \to \infty$ shows that

$$\gamma_0(\kappa) \underset{\kappa\to\infty}{=} \kappa - 2^{-1} k_0^2 a^2 \kappa^{-1} + O(k_0^4 a^4 \kappa^{-3}). \tag{28}$$

Then, introducing the function $\Omega(\kappa) = \gamma_0(\kappa) - \kappa$, and taking advantage of (17), (19), we arrive at the second-kind matrix equation (21), where now

$$\tilde{A}_{pn} = \int_0^{\infty} [\Omega(\kappa) + ik_0 aR] \phi_p(\kappa) \phi_n(\kappa) \kappa^{-1} d\kappa, \tag{29}$$

The equivalency between (22) and (29) follows from identity

$$K(s,s') - K_{st}(s,s') = \int_0^{\infty} \kappa \Omega(\kappa) J_1(\kappa s) J_1(\kappa s') d\kappa, \tag{30}$$

which enables obtaining one from another without the Hankel Transform. The same property holds for the right-hand parts.

Thus either way of building (21) requests analytical inversion of the static part of the corresponding IE. Here, to link MAR technique with the methods of [25–30,37], we note that the Jacobi polynomial $P_n^{(1,1/2)}(1-2s^2)$ reduces to the Chebyshev one, $U_{2n+1}(s)$, and the series like (27) in terms of functions (18) are called the Neumann series.

3.4. Log-singular IE for a VMD-excited resistive disk in free space

Consider now another auxiliary problem of a resistive disk in free space axisymmetrically excited by a VMD. Then the scattered field is sought as a single-layer potential:

$$E_\varphi(r,z) = \int_0^a j_\varphi(r') G^0(r,r',z,0)\, r'dr', \tag{31}$$

and GBC (3), (4) lead to the following IE for the unknown disk current, $j_\varphi(r)$:

$$ik_0^{-1}Rj_\varphi(r) + \int_0^a j_\varphi(r') G^0(r,r',0,0)\, r'dr' = ik_0^{-1}Z_0^{-1}E_\varphi^{in}(r), \tag{32}$$

One can verify that the kernel of (32) has a logarithmic singularity if $r \to r'$. Thus, for any $R \neq 0$ this is a Fredholm second-kind IE, which does not need an analytical regularization and can be discretized with any set of basis functions that are complete on $r \le a$. Here, one can take the functions that satisfy the edge condition and whose Hankel Transforms can be found analytically. Such basis functions, in terms of dimensionless coordinate s, are

$$\Psi_n(s) = \begin{cases} \chi_n s P_n^{(1,0)}\left(1-2s^2\right), & s \le 1, \\ 0, & s > 1, \end{cases} \tag{33}$$

where $n = 0, 1, \ldots$, $\chi_n = 2(n+1)^{1/2}$, $P_n^{(1,0)}(.)$ is the Jacobi polynomial. The corresponding Hankel Transform image is

$$\psi_n(\kappa) = \chi_n J_{2n+2}(\kappa), \quad 0 \le \kappa < \infty. \tag{34}$$

Hence, we expand the current and its image as

$$j_\varphi(s) = \sum_{n=0}^{\infty} y_n \Psi_n(s), \quad Y(\kappa) = \sum_{n=0}^{\infty} y_n \psi_n(\kappa), \tag{35}$$

respectively, and obtain a dual IE for the VMD-excited disk as

$$\begin{cases} \int_0^\infty Y(\kappa)\left[\gamma_0^{-1}(\kappa) + i(k_0 a)^{-1} R\right] J_1(\kappa s)\, d\kappa = i(k_0 a)^{-1} Z_0^{-1} E_r^{in}(s), & s \le 1 \\ \int_0^\infty Y(\kappa) J_1(\kappa s)\, d\kappa = 0, & s > 1 \end{cases}. \tag{36}$$

On discretizing (32) or (36) with the aid of (34) in the GM scheme, we obtain an infinite-matrix equation as

$$y_p + \sum_{n=0}^{\infty} y_n \widehat{A}_{np} = \widehat{B}_p, \quad p = 0, 1, 2 \ldots \infty. \tag{37}$$

Similarly to the VED case, here the matrix elements can be written in two equivalent ways:

$$\widehat{A}_{np} = -ik_0 a R^{-1} \int_0^1 \int_0^1 \Psi_p(s)\, \Psi_n(s')\, G^0(s,s')\, ss'dsds' \tag{38}$$

$$\widehat{A}_{np} = -ik_0 a R^{-1} \int_0^\infty \gamma_0^{-1}(\kappa)\kappa^{-1}\psi_p(\kappa)\psi_n(\kappa)d\kappa, \tag{39}$$

and the right-hand part column vector is determined by the excitation. Large-index behavior of the matrix elements is established as $O[(pn)^{1/2}(n^2+p^2)^{-1}]$ that leads to the conclusion of compactness of corresponding matrix operator, in the sense of space of number sequences $l_2\left\{y \in l_2 : \sum_{n=1}^{\infty} |y_n|^2 < \infty\right\}$.

4. Resistive disk on substrate excited by VED

4.1. Dual IEs for a resistive disk on substrate

Consider now a resistive disk-on-substrate shown in Fig. 1, i.e. excited by a VED located on the ground plane below the disk center. The current of such a feed is assumed to be

$$J_z^e(r',\varphi',z') = I^e l \delta(r')\delta(\varphi')r'^{-1}\delta(z'), \tag{40}$$

where $I^e l$ is the dipole moment, $\delta(.)$ is the Dirac delta.

Thanks to the equivalence discussed in Section 3A–C, we can avoid deriving a singular IE for the disk-on-substrate that needs using a layered-medium Green's function. Instead, tangential components of the electric and magnetic fields can be sought as inverse Hankel Transform integrals similarly to Eqs. (2)–(5) in [24]. By enforcing GBC (1), (2) on the

disk, continuity conditions on the substrate interface, and the PEC boundary condition on the ground plane, we derive the following dual IE:

$$\begin{cases} \int_0^\infty X(\kappa)\beta_R(\kappa, k_0, \varepsilon, h, a, R) J_1(\kappa s)\, d\kappa = \Pi(s), \quad s \le 1, \\ \int_0^\infty X(\kappa) J_1(\kappa s)\, d\kappa = 0, \ s > 1, \end{cases} \tag{41}$$

where $X(\kappa)$ is unknown image of the radial current on the disk, extended by zero value off the circle of radius a. The spectral weight function and excitation term are, respectively,

$$\beta_R(\kappa) = \gamma_0\gamma_\varepsilon \sinh(\gamma_\varepsilon h/a) D^{-1}(\kappa) + ik_0 aR; \tag{42}$$

$$\Pi(s) = v_0 \int_0^\infty \gamma_0(\kappa) D^{-1}(\kappa) J_1(\kappa s)\, \kappa^2 d\kappa, \tag{43}$$

$$D(\kappa) = \gamma_\varepsilon \sinh(\gamma_\varepsilon h/a) + \varepsilon\gamma_0 \cosh(\gamma_\varepsilon h/a), \tag{44}$$

where $v_0 = I^e l(2\pi)^{-1}$ and $\gamma_\varepsilon = (\kappa^2 - k_0^2 a^2 \varepsilon)^{1/2}$. Note that if $R = 0$, dual IE (41) reduce to the PEC-case ones of [9] and [24].

4.2. Matrix equation for a resistive disk on substrate

In order to transform dual IE (41) into an infinite matrix equation of the Fredholm second kind, we must inspect large-κ behavior of the function $\beta_R(\kappa)$. Expression (42) shows:

$$\beta_R(\kappa) = \zeta_0\kappa\left(1 - 2e^{-2\kappa\frac{h}{a}}\right) + ik_0 aR + \zeta_1 \frac{k_0^2 a^2}{\kappa} + O\left(\frac{k_0^4 a^4}{\kappa^3},\ \kappa e^{-4\kappa\frac{h}{a}}\right), \tag{45}$$

where $\zeta_0 = (1+\varepsilon)^{-1}$, $\zeta_1 = 2^{-1}\zeta_0(1+\varepsilon^2)$. Here it is seen that only the term corresponding to the *static limit of the single disk case* grows up as $O(\kappa)$, that is a singular behavior in Hankel-Transform sense. Further we introduce the function,

$$\Omega_R(\kappa) = \zeta_0^{-1}\kappa^{-1}[\gamma_0\gamma_\varepsilon \sinh(\gamma_\varepsilon h/a) D^{-1}(\kappa) - \kappa], \tag{46}$$

and observe that $\beta_R(\kappa) = \zeta_0\kappa[1 + \Omega_R(\kappa) + ik_0 aR]$. Finally, we expand the function $X(\kappa)$ similarly to (27) and retrace all the operations of the previous section to obtain the following equations:

$$x_p + \sum_{n=0}^{\infty} x_n A_{pn} = B_p, \quad p = 0, 1, 2 \ldots, \tag{47}$$

$$A_{pn} = \int_0^\infty \left[\Omega(\kappa) + ik_0 aR\kappa^{-1}\right] \phi_n(\kappa)\phi_p(\kappa) d\kappa, \tag{48}$$

$$B_p = v_0\zeta_0^{-1} \int_0^\infty D^{-1}(\kappa)\gamma_0(\kappa)\phi_p(\kappa)\kappa\, d\kappa. \tag{49}$$

One can easily show that the matrix operator with elements has finite l_2 norm and hence is compact, and the column-vector (49) also belongs to the space l_2. Therefore, is a Fredholm second-kind equation, which can be truncated and efficiently solved numerically. Fig. 2(a) demonstrates the behavior of the normalized truncation error, by the norm in l_2,

$$\delta(N) = \left(\sum_{n=0}^{N} \left|x_n^N - x_n^{N-1}\right|^2\right)^{1/2} \left(\sum_{n=0}^{N} \left|x_n^N\right|^2\right)^{-1/2}, \tag{50}$$

as a function of the matrix truncation number N. Provided that all intermediate operations have been done with superior accuracy, $\delta(N)$ starts rapid fall if $N > k_0 a\varepsilon^{1/2}$ and reaches machine precision with small N (the smaller a/h and R the better). This is something impossible for conventional MM algorithms, which hit a "numerical wall" after a few correct digits.

4.3. Filling in the matrix

As one can see, thanks to the Hankel Transform properties, the matrix elements can be reduced to one-dimensional integrals however on a semi-axis, see (39) and (48). Still, their numerical evaluation needs certain special efforts because (i) the integrand functions in (48) may have poles on the original contour of integration, between k_0 and $k_0\sqrt{\varepsilon}$, and (ii) the integration of improper integrals should take a reasonable computation time. Fortunately, both circumstances have been already considered in detail in preceding works (see, for instance, [39,40] and also [27,28]).

The remedy to the former trouble is the deformation of the contour by shifting it from the real axis to the upper halfplane of the complex plane of κ, on a finite interval (see Fig. 3 of [24]). Due to the Jordan lemma and the fact that the first quadrant is free of the poles of $\Omega_R(\kappa)$, such a deformation is safe and the integration result is the same as along the original path's interval.

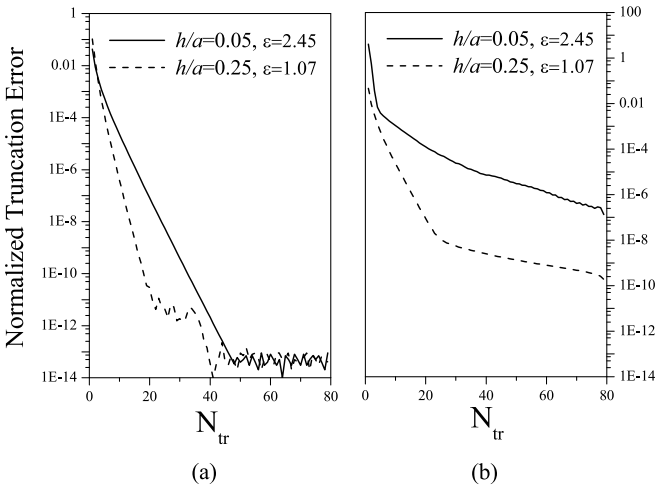

Fig. 2. Truncation error at $a/\lambda_0 = 0.5$ for (a) resistive disk-on-substrate scatterer, $R = 0.05$ and (b) thin dielectric disk, $\varepsilon_d = 152$, $\tan\delta = 0.001$, $b/a = 0.001$.

The latter trouble, i.e. the computation of the remaining "tail" integral along the positive real axis of κ, reduces to a proper choice of the upper limit, which depends on the desired accuracy. This operation can be greatly accelerated by the so-called asymptotic-extraction technique first introduced in [39,40] and widely used today. This implies subtraction, from the integrand, several first terms of the inverse-power expansion of $\Omega_R(\kappa)$ that can be integrated explicitly with the aid of the Weber–Shafheitlin formulas [41]. Then, the remainder integrand decays as κ^{-8} if $\kappa \to \infty$ and hence the integration limit becomes small even if the desired accuracy is requested to be at machine precision, like it is for the curves in Fig. 2(a).

Additionally, the time of filling in the matrix (47) is reduced by using the recurrence formulas for the Bessel functions [23,24] that allows computing only $3N$ matrix elements (48) instead of N^2.

Similar asymptotic acceleration techniques are also used to speed up the computation of the right-hand-part coefficients (49). Moreover, this technique can be applied to the efficient computation of the field components in the near zone of the disk.

5. Thin disk on substrate dielectric antenna excited by VED

5.1. Coupled set of dual IEs for a thin dielectric disk on substrate

Consider now the case of a thin disk-on-substrate scatterer. Following the same scheme as in Sections 3 and 4, we use GBC (3), (4), extend the effective currents on the disk with zero values off the circle of radius a, and introduce the Hankel Transform images of these currents and the modal Green's function. This enables us to obtain a coupled set of dual IEs,

$$\begin{cases} \int_0^\infty \left[X(\kappa)\beta_R^d(\kappa) + Y(\kappa)\sigma(\kappa)\right] J_1(\kappa s)\, d\kappa = \Pi_x(s), \ s \le 1 \\ \int_0^\infty X(\kappa) J_1(\kappa s)\, d\kappa = 0, \ s > 1 \end{cases} \tag{51}$$

$$\begin{cases} \int_0^\infty \left[Y(\kappa)\beta_S^d(\kappa) + X(\kappa)\sigma(\kappa)\right] J_1(\kappa s)\, d\kappa = \Pi_y(s), \ s \le 1 \\ \int_0^\infty Y(\kappa) J_1(\kappa s)\, d\kappa = 0, \ s > 1 \end{cases} \tag{52}$$

where the function Π_x is the same as in (43), and

$$\beta_R^d(\kappa) = \gamma_0\gamma_\varepsilon \sinh(\gamma_\varepsilon h/a) D^{-1}(\kappa) - ik_0 a R_d, \tag{53}$$

$$\beta_S^d(\kappa) = \Omega_S(\kappa) + iS_d(k_0 a)^{-1}, \tag{54}$$

$$\Omega_S(\kappa) = \varepsilon \cosh(\gamma_\varepsilon h/a) D^{-1}(\kappa), \tag{55}$$

$$\sigma(\kappa) = 2^{-1}[\gamma_\varepsilon \sinh(\gamma_\varepsilon h/a) - \gamma_0\varepsilon \cosh(\gamma_\varepsilon h/a)] D^{-1}(\kappa), \tag{56}$$

$$\Pi_y(s) = -v_0 \int_0^\infty D^{-1}(\kappa) J_1(\kappa s)\, \kappa^2 d\kappa. \tag{57}$$

Unlike $\beta_R^d(\kappa)$, the expansion of $\beta_S^d(\kappa)$ at $\kappa \to \infty$ starts from a constant term that shows non-singular nature of dual IE (50). One can also notice that dielectric-disk dual IEs reduce to resistive-disk ones if $S_d^{-1} = 0$ that entails $Y(\kappa) = 0$.

5.2. Matrix equation for a thin dielectric disk on substrate

In order to reduce (51), (52) to the Fredholm second-kind matrix equation by means of MAR combined with GM, we should find appropriate sets of basis functions. Analysis shows that Eq. (53) has the same features as dual IE for the VED-excited resistive disk, and (52) is similar to the VMD-case. Then it is clear that $X(\kappa)$ and $Y(\kappa)$ should be expanded in the Neumann series of functions (18) and (34), respectively. This leads to the following block-type (2×2) matrix equation:

$$\begin{cases} x_p + \sum\limits_{n=0}^{\infty} x_n A_{np} + \sum\limits_{n=0}^{\infty} y_n F^x_{np} = B^x_p, \quad p = 0, 1, 2, \dots \\ y_p + \sum\limits_{n=0}^{\infty} x_n F^y_{np} + \sum\limits_{n=0}^{\infty} y_n C_{np} = B^y_p, \quad p = 0, 1, 2, \dots \end{cases} \tag{58}$$

where x_n and y_n are unknowns, A_{pn} and B^x_p are determined by where R is replaced with R_d and (49), respectively,

$$F^x_{np} = (\varepsilon + 1)\int_0^{\infty} \sigma(\kappa)\phi_p(\kappa)\psi_n(\kappa)\kappa^{-1} d\kappa, \tag{59}$$

$$F^y_{np} = \tau(1+\varepsilon)^{-1} F^y_{np} \quad \tau = ik_0 a S_d^{-1}, \tag{60}$$

$$C_{np} = -\tau\int_0^{\infty} \Omega_S(\kappa)\psi_p(\kappa)\psi_n(\kappa)\kappa^{-1} d\kappa, \tag{61}$$

$$B^y_p = v_0\tau\int_0^{\infty} D^{-1}(\kappa)\psi_p(\kappa)\kappa\, d\kappa. \tag{62}$$

The matrices of each block of (58) have bounded l_2-norms, and right-hand parts belong to l_2. Hence, each block can be truncated to the order N and then (60) can be solved in the same way as for a resistive disk. Dashed curves in Fig. 2(b) show truncation error, in the sense of the norm of the space $l_2^2 = l_2 \otimes l_2$, as a function of N. As seen, for dielectric disk the error starts a fall down if $N > k_0\varepsilon^{1/2}a$ with the rate determined by h/a and the largest of the values R_d and S_d^{-1}.

6. Numerical results

The formulas for computing the radiation characteristics of resistive and dielectric disk-on-substrate antennas are similar to those for PEC disk antenna [24]. The only difference is the presence of losses in imperfect disk. Therefore, the power radiated into the free half-space as a spherical wave and the power absorbed in a thin dielectric disk are, respectively,

$$\frac{P_{rad}}{P_0} = 6\pi^2\int_0^{\pi/2} \left[|X(k_0\sin\alpha)|^2 + |Y(k_0\sin\alpha)|^2\right]\sin 3\alpha\, d\alpha, \tag{63}$$

$$\frac{P_{abs}}{P_0} = -\frac{6\pi^2}{k_0^2a^2}\left[ReR_d\int_0^{\infty} |X(\kappa)|^2\frac{d\kappa}{\kappa} + \frac{ReS_d}{k_0^2a^2}\int_0^{\infty} |Y(\kappa)|^2\frac{d\kappa}{\kappa}\right], \tag{64}$$

where $P_0 = 2\pi v_0^2 Z_0 k_0^2/3$ is the power radiated by a VED into the free half-space. For a resistive-disk scatterer, the second term in the brackets in (64) is absent.

Note that expression (64) is the same as the absorption resistance of lossy dielectric disk, normalized by the radiation resistance of VED in the free half-space. The radiation efficiency is defined as

$$\eta = P_{rad}/(P_{rad} + P_{sw} + P_{abs}) \tag{65}$$

where P_{sw} is the power taken to infinity along the substrate by the surface waves of the substrate [24]. Throughout the computations, we keep the integration and matrix-truncation errors to be lower than 10^{-8} and 10^{-5}, respectively, and check the power balance (i.e. Poynting theorem), which is satisfied at the 10^{-8} level.

6.1. Radiation characteristics of resistive disk antenna

The plots in Figs. 3–6 show electromagnetic performance of a resistive disk antenna on a thin substrate for different disk resistivities. The frequency dependences of the normalized space and surface-wave powers are depicted in Figs. 3 and 4.

Note that in the studied frequency band only the principal surface wave of the substrate can propagate. As we can see, behavior of the far-field characteristics is generally similar to the PEC disk antenna. So far as resistivity is small, sharp maxima are observed at resonant frequencies. Additionally, the surface-wave power has sharp minima at the frequencies where the so-called surface-wave suppression condition is satisfied [42]. If the disk material is a poor conductor, then the resonances are spoiled and the power curves versus the frequency get smoother.

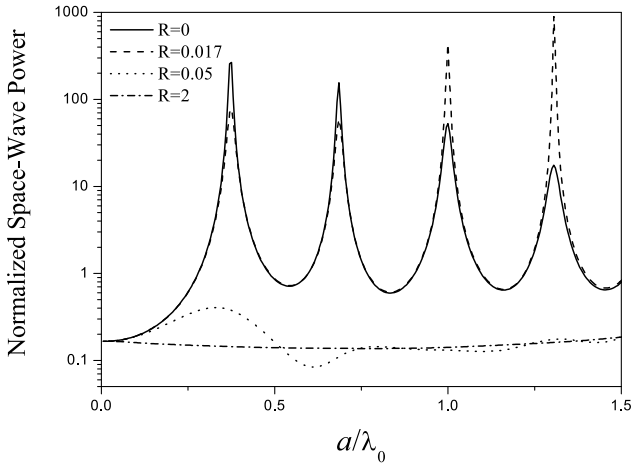

Fig. 3. Normalized space-wave power versus normalized disk radius for a resistive disk on a thin substrate. $\varepsilon = 2.45$, $h/a = 0.05$.

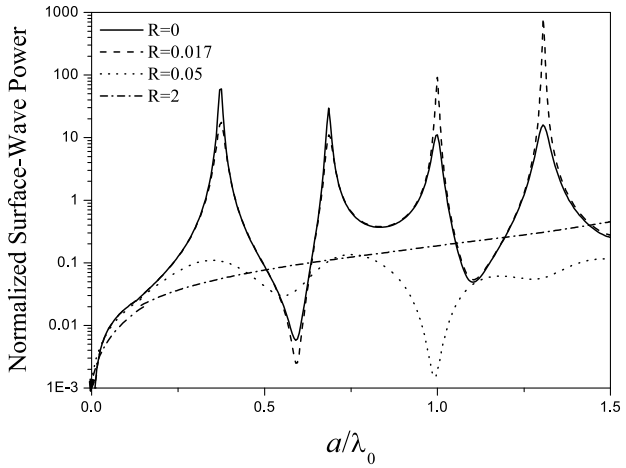

Fig. 4. Normalized surface-wave power versus normalized disk radius for a resistive disk on a thin substrate. $\varepsilon = 2.45$, $h/a = 0.05$.

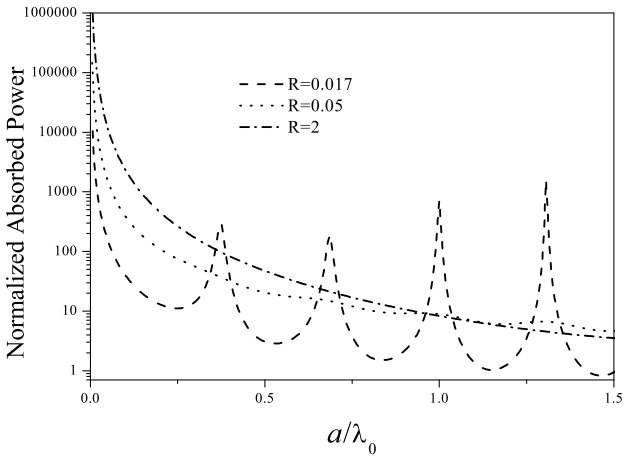

Fig. 5. Normalized absorbed power versus normalized disk radius for a resistive disk on a thin substrate. $\varepsilon = 2.45$, $h/a = 0.05$.

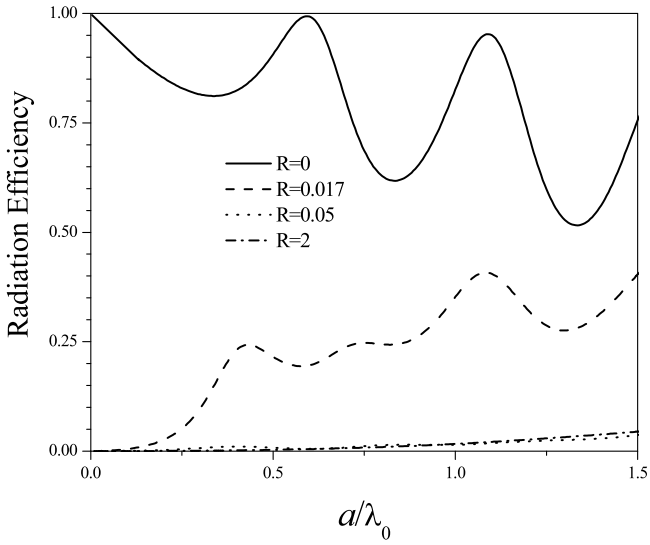

Fig. 6. Radiation efficiency versus normalized disk radius for a resistive disk on a thin substrate. $\varepsilon = 2.45$, $h/a = 0.05$.

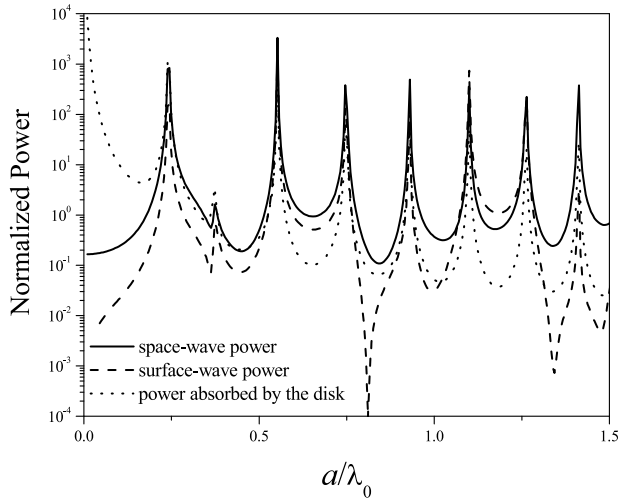

Fig. 7. Power characteristics versus the normalized disk radius for a dielectric disk on a thin substrate. $\varepsilon = 2.45$, $h/a = 0.05$, $\varepsilon_d = 152$, $\tan\delta = 0.001$, $b/a = 0.01$.

A new feature is the absorption in resistive disk that has maxima in the resonances (Fig. 5). Due to normalization applied the curves go down if the frequency is increased, although the absorption itself goes up. In the low-frequency limit, P_{abs} falls down less rapidly than the normalization value in (63) (i.e., P_0) and therefore the curves tend to infinity.

Eventually, Fig. 6 demonstrates a comparison of radiation efficiencies of the PEC and resistive disks on a thin dense substrate. The main effect of $R \neq 0$ is that the presence of even small losses causes the radiation efficiency depression at $a/\lambda_0 \to 0$. Such a behavior is in contrast to the PEC disk models, where efficiency of radiation tends to 100% at zero frequency. Note that here the radiation efficiency is generally greater than in the case of a thin high-permittivity substrate, although the power radiated in the first resonance is considerably lower.

6.2. Radiation characteristics of thin dielectric disk antenna

Figs. 7 and 8 demonstrate the performance of thin-disk dielectric antenna made of very high-ε material and built on a thin dense substrate and a thick foam-like one, respectively.

Comparison of Figs. 7 and 3–5 shows that the structure of the resonances changes considerably, with new resonances brought by a very dense dielectric disk. In resonances, the radiated power is higher than for a PEC disk, apparently thanks

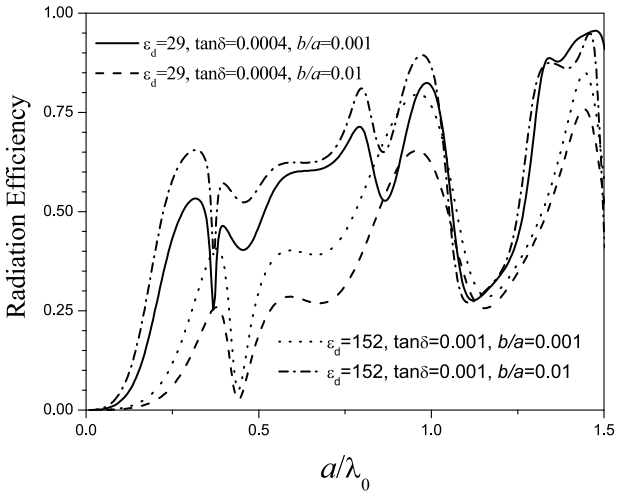

Fig. 8. Radiation efficiency versus normalized radius for a dielectric disk on a thin substrate. $\varepsilon = 2.45$, $h/a = 0.05$.

to the partial transparency. What is remarkable, the radiation efficiency does not gradually fall down with increasing the frequency but displays bands of high values (Fig. 8).

7. Conclusions

We have presented the MAR technique based on the analytical inversion of the static part of the isolated disk problem and applied to the imperfect thin disk-on-substrate antenna analysis. This implies the use of the generalized two-side boundary conditions, which lead to the hyper-singular or logarithmic-singular IEs or, equivalently, to the dual IEs in the Hankel Transform domain. It must be noted that previously published works dealt exclusively with PEC disk configurations. Unlike previously used techniques, we perform regularization of IEs using the Galerkin-method diagonalization with the static-case eigenfunctions or by the inverse Hankel Transform, depending on the IE properties. This procedure can be also considered as analytical preconditioning, which guarantees convergence of resulting matrix equations with respect to the truncation order and makes the numerical analysis very economic and accurate. With the aid of such sophisticated numerical instrument, we have quantified important for applications feature of improved radiation efficiency of imperfect disk-on-substrate antennas.

CRediT authorship contribution statement

Nataliya Y. Saidoglu: Formal analysis, Investigation, Software, Validation, Visualization, Writing - original draft. **Alexander I. Nosich:** Conceptualization, Methodology, Supervision, Writing - review & editing.

References

[1] D.M. Pozar, D.H. Shaubert (Eds.), Microstrip Antennas, IEEE Press, NY, 1995.
[2] J. Huang, Circularly polarized conical patterns from circular microstrip antennas, IEEE Trans. Antennas and Propagation AP-32 (9) (1984) 991–994.
[3] L. Economou, R.J. Langley, Circular microstrip patch antennas on glass for vehicle applications, IEE Proc., Microw. Antennas Propag. 145 (5) (1998) 418–420.
[4] C.-Y. Huang, Microstrip antenna with lossy patch, Microw. Opt. Technol. Lett. 15 (2) (1998) 228–230.
[5] A.A. Kishk, M.R. Zanoubi, D. Kajfez, A numerical study of a dielectric disk antenna above grounded dielectric surface, IEEE Trans. Antennas and Propagation 41 (6) (1993) 813–821.
[6] S.N. Makarov, V. Iyer, A narrowband patch antenna with a dielectric patch, in: Proc. IEEE Int. Symp. Antennas Propagat, IEEE APS-2008, San Diego, 2008, art. no 4620011.
[7] H.W. Lai, K.-M. Luk, K.W. Leung, Dense dielectric patch antenna - a new kind of low-profile antenna element for wireless communications, IEEE Trans. Antennas and Propagation 61 (8) (2013) 4239–4245.
[8] T. Itoh, R. Mittra, Analysis of a microstrip disk resonator, Arch. Elektron. Ubertrat. Techn. 27 (11) (1973) 456–458.
[9] W.C. Chew, J.A. Kong, Resonances of the axial-symmetric modes in microstrip disk resonators, J. Math. Phys. 21 (6) (1980) 582–591.
[10] W.C. Chew, J.A. Kong, Analysis of a circular microstrip antenna with a thick dielectric substrate, IEEE Trans. Antennas and Propagation 29 (1) (1981) 68–76.
[11] S. Yano, A. Ishimaru, A theoretical study of the input impedance of a circular microstrip disk antenna, IEEE Trans. Antennas and Propagation 29 (1) (1981) 77–83.
[12] T. Itoh, K. Araki, Hankel transform domain analysis of open circular microstrip radiation structures, IEEE Trans. Antennas and Propagation 29 (1) (1981) 84–89.

[13] J. Mosig, R.L. Hall, F. Gardiol, Numerical analysis of microstrip patch antennas, in: J.R. James, P.S. Hall (Eds.), in: Handbook of Microstrip Antennas, vol. 1, Peter Peregrinus, London, 1989, chap. 8.
[14] D.G. Dudley, Error minimization and convergence in numerical methods, Electromagnetics 5 (2) (1985) 89–97.
[15] G.L. Hower, R.G. Olsen, J.D. Earls, J.B. Schneider, Inaccuracies in numerical calculation of scattering near natural frequencies of penetrable objects, IEEE Trans. Antennas and Propagation 41 (7) (1993) 982–986.
[16] G. Bouchitte, R. Petit, On the concepts of a perfectly conducting material and of a perfectly conducting and infinitely thin screen, Radio Sci. 24 (1) (1989) 13–26.
[17] E. Bleszynski, M. Bleszynski, T. Jaroszewicz, Surface integral equations for electromagnetic scattering from impenetrable and penetrable sheets, IEEE Antennas Propag. Mag. 35 (6) (1993) 14–25.
[18] I.-S. Koh, K. Sarabandi, A new approximate solution for scattering by thin disks of arbitrary shape and size, IEEE Trans. Antennas and Propagation 53 (6) (2005) 1920–1926.
[19] I.-T. Chiang, W.-C. Chew, Thin dielectric sheet simulation by surface integral equation using modified RWG and pulse bases, IEEE Trans. Antennas and Propagation 54 (7) (2006) 1927–1934.
[20] A.I. Nosich, Method of analytical regularization in the wave-scattering and eingenvalue problems: foundations and review of solutions, IEEE Antennas Propag. Mag. 41 (3) (1999) 34–49.
[21] V.B. Sologub, Short-wave asymptotic behaviour of the solution of the problem of diffraction by a circular disk, USSR J. Comput. Math. Mathem. Phys. 12 (2) (1972) 135–164.
[22] B.A. Dunai, A.V. Lugovoi, V.B. Sologub, Scattering of electromagnetic waves by a disk located at the boundary of a dielectric half-space, Sov. Phys. Techn. Phys. 20 (10) (1975) 1396–1398.
[23] A.N. Khizhnyak, S.S. Vinogradov, Scalar plane-wave diffraction by finite number of equidistant coaxial circular disks, Microw. Opt. Technol. Lett. 17 (5) (1998) 328–332.
[24] N.Y. Bliznyuk, A.I. Nosich, A.N. Khizhnyak, Accurate computation of a circular-disk antenna axisymmetrically excited by an electric dipole, Microw. Opt. Technol. Lett. 25 (3) (2000) 211–216.
[25] G. Panariello, F. Schettino, L. Verolino, R. Araneo, S. Celozzi, Analysis of microstrip antennas by means of the regularization via Neumann series, in: Review of Radio Science: 1999-2002, Wiley-IEEE Press, 2002, pp. 111–124.
[26] F. Di Murro, M. Lucido, G. Panariello, F. Schettino, Guaranteed-convergence method of analysis of the scattering by an arbitrarily oriented zero-thickness PEC disk buried in a lossy half-space, IEEE Trans. Antennas and Propagation 63 (8) (2015) 3610–3620.
[27] M. Lucido, G. Panariello, F. Schettino, Scattering by a zero-thickness PEC disk: a new analytically regularizing procedure based on Helmholtz decomposition and Galerkin method, Radio Sci. 52 (1) (2017) 2–14.
[28] G. Lovat, P. Burghignoli, R. Araneo, S. Celozzi, A. Andreotti, D. Assante, L. Verolino, Shielding of a perfectly conducting circular disk: exact and static analytical solution, Progr. Electromagn. Res. C 95 (2019) 167–182.
[29] M. Lucido, F. Schettino, G. Panariello, Scattering from a thin resistive disk: a guaranteed fast convergence technique, IEEE Trans. Antennas and Propagation 68 (2020) in press.
[30] G. Lovat, P. Burghignoli, R. Araneo, S. Celozzi, A. Andreotti, D. Assante, L. Verolino, Shielding of an imperfect metallic thin circular disk: exact and low-frequency analytical solution, Progr. Electromagn. Res. C 98 (2020) in press.
[31] V.S. Bulygin, Y.V. Gandel, A.I. Nosich, Nystrom-type method in three-dimensional electromagnetic diffraction by a finite PEC rotationally symmetric surface, IEEE Trans. Antennas and Propagation 60 (11) (2012) 4710–4718.
[32] V.S. Bulygin, Y.V. Gandel, T.M. Benson, A.I. Nosich, Full-wave analysis and optimization of a TARA-like shield-assisted paraboloidal reflector antenna using a nystrom-type method, IEEE Trans. Antennas and Propagation 61 (10) (2013) 4981–4989.
[33] J.L. Tsalamengas, Quadrature rules for weakly singular, strongly singular, and hypersingular integrals in boundary integral equation methods, J. Comput. Phys. 303 (12) (2015) 498–513.
[34] A.I. Nosich, R. Sauleau, Simulation of graphene-disk antenna with axially symmetric excitation using MAR and orthogonal polynomials, in: Proc. Int. Conf. Transparent Optical Networks, ICTON-2016, Trento, 2016, We.B6.3.
[35] A.I. Nosich, Radiation conditions, limiting absorption principle, and general relations in open waveguide scattering, J. Electromagn. Waves Appl. 8 (3) (1994) 329–353.
[36] I.M. Braver, P.S. Fridberg, K.L. Garb, I.M. Yakover, The behavior of the electromagnetic field near the edge of a resistive half-plane, IEEE Trans. Antennas and Propagation 36 (12) (1988) 1760–1768.
[37] V. Losada, R.R. Boix, M. Horno, Resonant modes of circular microstrip patches on multilayered substrates, IEEE Trans. Microw. Theory Tech. 47 (4) (1999) 488–498.
[38] I.S. Gradstein, I.M. Ryzhik, Tables of Integrals, Series and Products, Academic Press, London, 1994.
[39] S.O. Park, C.A. Balanis, Closed-form asymptotic extraction method for coupled microstrip lines, IEEE Microw. Guid. Wave Lett. 7 (3) (1997) 84–86.
[40] S. Amari, R. Vahldieck, J. Bornemann, Using selective asymptotics to accelerate dispersion analysis of microstrip lines, IEEE Trans. Microw. Theory Tech. 46 (7) (1998) 1024–1027.
[41] M. Abramovitz, I.A. Stegan, Handbook of Mathematical Functions, Dover, NY, 1979.
[42] D. Jackson, J.T. Williams, A.K. Bhattacharyya, R.L. Smith, et al., Microstrip patch designs that do not excite surface waves, IEEE Trans. Antennas and Propagation 41 (10) (1993) 1026–1037.